
Induced Modularity and Community Detection for Functionally Interpretable Reinforcement Learning

Anna Soligo

Pietro Ferraro

David Boyle

Imperial College London

Abstract

Interpretability in reinforcement learning is crucial for ensuring AI systems align with human values and fulfill the diverse related requirements including safety, robustness and fairness. Building on recent approaches to encouraging sparsity and locality in neural networks, we demonstrate how the penalisation of non-local weights leads to the emergence of functionally independent modules in the policy network of a reinforcement learning agent. To illustrate this, we demonstrate the emergence of two parallel modules for assessment of movement along the X and Y axes in a stochastic Minigrid environment. Through the novel application of community detection algorithms, we show how these modules can be automatically identified and their functional roles verified through direct intervention on the network weights prior to inference. This establishes a scalable framework for reinforcement learning interpretability through functional modularity, addressing challenges regarding the trade-off between completeness and cognitive tractability of reinforcement learning explanations.

1 INTRODUCTION

Deep reinforcement learning (RL) has emerged as a powerful approach for improving performance in complex decision making domains. Learning policies directly from interactions can offer increased flexibility and improved performance, whilst avoiding the challenges of designing effective cost functions and planning strategies faced by classical model-based control approaches (Song et al., 2023). A growing body of research is demonstrating the potential for RL to have positive impacts in diverse real-world domains, from

battery manufacturing (Lu et al., 2020) to the design of medical treatment regimes (Coronato et al., 2020): applications which directly implicate on critical issues such as climate-change and human-health. However, such broad implications also introduce societal risks, and the application of RL raises wide-ranging concerns related to topics of safety, reliability, privacy and bias, among others. For this reason, it becomes crucial that the behaviour of RL agents can be properly characterised, to the extent that it can be reasonably verified that their impacts will positively align with human values. As reflected in the EU’s AI ethics guidelines: systems must allow for human oversight, accountability and transparency (European Commission and High-Level Expert Group on AI, 2019).

However, there are fundamental challenges to achieving this, and current RL systems rarely afford sufficient levels of interpretability to fulfill these three requirements. Central to this is the ambiguity regarding what constitutes an acceptable ‘explanation’ of a model. A balance must be struck between the scope and detail of an explanation and its suitability for a human audience. Human understanding of an explanation must be considered to ensure its utility, whilst also avoiding incompleteness that risks leaving room for subjective interpretations. Lipton (2016) considers this concept of a tractable explanation under the term of ‘simulatability’: the idea that a human can, in reasonable time, take a model input and explanation and predict its output. He pairs this with the parallel notion of ‘decomposability’, which suggests that the constituent components of a model should be individually interpretable. These notions are echoed by Doshi-Velez and Kim (2017) through the concept of ‘cognitive chunks’, emphasising their relevance to human processing. Questions arise regarding how the size, number, organisation and interactions of these relate to whether a model or explanation can be considered understandable.

In this work we address these challenges by taking a modular perspective to interpretability, drawing inspi-

ration from cognitive science. Cognition is frequently viewed as consisting of semi-encapsulated modules with distinct functions (Fodor, 1985; Sternberg, 2011) and modular processing is prevalent in both conscious decision making and the physical structures of the brain (Eppe et al., 2022; Gazzaniga et al., 2018). Given the pervasive need to consider human comprehension of model explanations, this suggests interpretability through a modular lens is a promising approach to understanding RL decision making at a tractable level of abstraction.

1.1 Contributions

Leveraging this concept of interpretability at the level of functional modules, our work makes the following contributions:

- We build on recent bio-inspired algorithms for encouraging locality in neural networks (Achterberg et al., 2023; Liu et al., 2023; Margalit et al., 2024) and demonstrate that the penalisation of non-local weights encourages the emergence of semi-encapsulated functional modules in the policy network of an RL agent: a level of decomposition which we suggest strongly aligns with human decision making frameworks.
- We show how the application of community detection methods, based on the Louvain algorithm and spectral analysis of the adjacency matrix, allows for the automatic detection of modules within neural networks. This demonstrates the potential to automate and scale modular interpretability.
- Finally, drawing on techniques from mechanistic interpretability, we demonstrate how direct intervention on network weights prior to inference enables the characterisation of detected modules, offering a verifiable interpretation of their functionality.

We show interactive graphs of modular RL networks and animations of their functional behavior on the project page:

<https://sites.google.com/view/functionally-interpretable-rl>

2 BACKGROUND AND RELATED WORKS

Following Glanois et al. (2024), and to avoid confusion arising from the inconsistent use of terms in the literature, we define interpretability as a passive model quality denoting the extent to which a model’s inner

workings can be examined and understood. We distinguish this from explainability, which we define as an external understanding of model behaviour that arises from active, generally post-hoc, attempts at explaining the decision making process. Interpretability and explainability thus present two different paths to obtaining information that can be used to generate explanations for model behaviour. Although post-hoc explainability methods can offer improved flexibility and scalability compared to intrinsic interpretability approaches, their lack of grounding in model internals raises concerns regarding the potentially misleading and subjective nature of the resulting explanations (Adebayo et al., 2018; Atrey et al., 2019).

In this work we take a direct interpretability approach by aiming to learn an intrinsically more interpretable model architecture. Decision trees are a prevalent existing approach to achieving this and can be used to learn Q-values or policies. Although their classical implementation using boolean decision variables is not differentiable, recent work on ‘soft decision trees’ enables efficient reinforcement learning through gradient descent (Silva et al., 2020). Symbolic equations offer an alternative intrinsically interpretable architecture, and diverse methods exist to generate effective RL policies in this form. For instance, using genetic programming to efficiently search a space of function trees (Hein et al., 2017) or learning a recurrent neural network (RNN) to directly generate policy equations (Landajuela et al., 2021). Beyond mathematical operators, policies have been learnt as weighted combinations of first order logic rules, from which natural language explanations can be extracted (Jiang and Luo, 2019).

These approaches demonstrate a reliance on making fundamental model architecture changes to improve interpretability, which leads to issues regarding scalability and performance. Although the components of the described methods, such as formulaic policies, can theoretically scale to complex scenarios, this rapidly becomes computationally prohibitive, even when classically discrete approaches are relaxed to be continuous or an indirect policy distillation approach is adopted (Glanois et al., 2024). Moreover, scaling these architectures to improve performance compromises their interpretability: a decision tree with an intractable number of nodes, for example, may be no more interpretable than a network with an intractable number of neurons.

Tangentially, the field of mechanistic interpretability takes a bottom up approach to reverse-engineering networks, particularly large language models. Notably this can involve the identification of ‘circuits’: computational sub graphs within a network which perform

specific tasks (Wang et al., 2022). We share this task-level focus, but rather than attempting interpretability at the level of computations, as per the aforementioned approaches, we instead characterise higher-level collections of neurons.

These collections of neurons, or ‘modules’, can be considered in terms of both their topological and functional modularity. Topological (or structural) modules are communities of neurons that are densely interconnected by network weights, while being sparsely connected to external neurons. Conversely, functional modules are sets of neurons which together perform specific tasks with a level of independence from the remainder of the network. A number of neural network architectures exhibit principles of modularity. At the data level, manual or learnt decomposition of the domain can parallelise processing, for example by partitioning regions of an image to be independently processed by CNNs (Zhang et al., 2014). Within networks, sequential structural modularity can be seen in the repeated-block structure of transformers, which is additionally parallelised in a functional manner in multi-modal architectures (He et al., 2021).

For the purpose of interpretability, we are interested in functional modularity, for which topological modularity is a necessary but not sufficient condition (Amer and Maul, 2019). This is approached by policy tree approaches to hierarchical RL, which decompose decision making into sub policies (Pateria et al., 2021). However, these are limited to a predefined level of decomposition and only afford interpretability when discernible sub-behaviours, such as motor primitives (Merel et al., 2018), are explicitly learnt based on prior knowledge.

Functional modularity in the brain arises alongside its ‘small-world’ architecture: a combination of high clustering and short average path length hypothesised to have evolved to satisfy spatial and energy constraints (Margalit et al., 2024). Recently, several works have investigated the impacts of applying analogous constraints to neural networks. Achterberg et al. (2023) spatially embed an RNN and penalise its connections relative to their length, demonstrating high energy efficiency and a level of functional clustering in a one-step inference task. Concurrently, Margalit et al. (2024) introduced a training loss to encourage correlation between local activations and applied this to convolutional layers projected onto simulated cortical sheets. While these studies apply bio-inspired training for the purpose of advancing neuro-scientific understanding and modelling, Liu et al. (2023) employ similar techniques to improve the interpretability of neural network visualisations. They demonstrate that their ‘brain inspired modular training’ approach, which cou-

ples length-relative weight penalisation with neuron relocation during training, reveals structures within tasks such as regression to symbolic mathematical formulae. Building on these findings, we extend this ‘small-world’ approach to an RL context to encourage functional modularity. We further propose methods for automatic detection and characterisation of the resulting modules, enabling scalable interpretability in a decision making context.

3 METHODS

3.1 Proximal Policy Optimisation (PPO)

We use the standard RL formalism for an agent interacting with a fully observable environment. The environment is described by the set of states \mathcal{S} , set of discrete actions \mathcal{A} , reward function $r : \mathcal{S} \times \mathcal{A} \rightarrow \mathbb{R}$, discount factor $\gamma \in [0, 1]$, and transition probabilities $p(s_{t+1}|s_t, a_t)$. The policy $\pi_\theta : \mathcal{S} \rightarrow \mathcal{A}$ generates a probability distribution over actions, from which an action a_t is sampled at each time step t . Each action results in a reward $r_t = r(s_t, a_t)$ and an updated environment state s_{t+1} . The return of a state-action pair is defined as the discounted sum of future rewards, $R_t = \sum_{i=t}^{\infty} \gamma^{i-t} r_i$, and the expected return is given by the action-value function $Q^\pi(s_t, a_t) = \mathbb{E}[R_t | s_t, a_t]$.

We apply PPO (Schulman et al., 2017) due to its stability and simplicity. As a policy-gradient method, PPO directly learns the parameterised policy function, the actor, by estimating the gradient of the expected return with the respect to the policy parameters. The generalised advantage estimator (GAE) is used to determine the advantage of taking an action a_t over alternative actions in state s_t . This advantage is defined as $A(s_t, a_t) = Q(s_t, a_t) - V(s_t)$, where $V^\pi(s_t) = \mathbb{E}[R_t | s_t]$: the state-value function approximated by a critic network. The GAE value is clipped to constrain the magnitude of the policy change at each learning step and prevent large changes which may lead to performance collapse.

3.2 Spatially Aware Regularisation

L1 regularisation encourages sparsity by penalising the absolute values of the model parameters. Following Achterberg et al. (2023); Liu et al. (2023), we extend this to encourage local connectivity by projecting the neural network into Euclidian space and scaling L1 weight penalties by the distance between the neurons they connect.

For a network with L weight layers and $L + 1$ neuron layers, we denote neuron layers as \mathbf{N}_l where $l \in \{0, 1, \dots, L\}$ and weight layers as \mathbf{W}_l where

$l \in \{1, \dots, L\}$. For our fully connected networks, $\mathbf{W}_l \in \mathbb{R}^{N_{l-1} \times N_l}$ and each weight w_l^{ij} connects the i^{th} neuron in N_{l-1} with the j^{th} neuron in N_l . The dimension of the neuron layer N_l is n_l , such that n_0 and n_L represent the dimensions of the input features and discrete action space respectively.

All neurons n_l^i in N_l share a y coordinate: $y_l^i := y_l, i \in \{1, \dots, n_l\}$. Initial x coordinates are defined as uniformly spaced along this axis such that $x_l^i = \frac{i}{n_l}$. A weighting factor, λ_{cc} , scales the connection cost loss in each layer to give the total network connection cost, L_{cc} defined in Equation 1.

$$L_{cc} = \lambda_{cc} \sum_{l=1}^L \sum_{i=1}^{n_{l-1}} \sum_{j=1}^{n_l} \|p_{l-1}^i - p_l^j\| |w_l^{ij}| \quad (1)$$

where

$$p_l^i = [x_l^i, y_l]$$

Note that if all neuron pairs are equidistant (i.e., $\|p_{l-1}^i - p_l^j\|$ is a constant) L_{cc} reduces to L1 sparsity.

To further encourage locality, neurons positions are systematically relocated during training in a manner that minimises the total connection cost L_{cc} of the network, as proposed by Liu et al. (2023). At a fixed update interval and for every hidden layer, the weighted degree of each neuron is calculated as the sum of its incoming and outgoing weights:

$$w(n) = \sum |w(n)_{in}| + \sum |w(n)_{out}| \quad (2)$$

The $k = 10$ neurons with highest $w(n)$ are selected for position optimization. For each candidate neuron n_c , the relocation algorithm:

1. Computes the baseline connection cost CC_0 for the current configuration, based on Equation 1.
2. For every other neuron n_i in the same layer as n_c , calculates an updated connection cost CC_i obtained by swapping the positions of n_c and n_i
3. Identifies the swap partner n_s that yields $\min(CC_i)$
4. If $\min(CC_i) < CC_0$, executes the position swap between n_c and n_s

3.3 Minigrid

We conduct experiments using the dynamic obstacles Minigrid environment shown in Figure 1 (Chevalier-Boisvert et al., 2023). This consists of an agent, goal and three ‘ball’ obstacle entities randomly initialised in a 4x4 grid, which is encoded into a symbolic observation of entity coordinates relative to the agent. The action space consists of left, right, up and down steps and

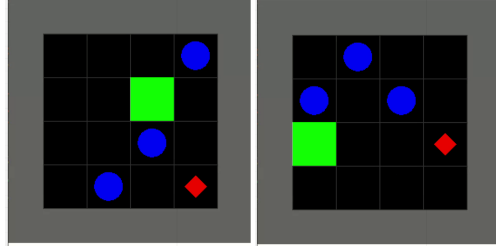


Figure 1: Example Environment Frames Showing the Agent (Red), Dynamic Obstacles (Blue) and Goal (Green).

each ball takes one random step per agent step. Following the NAVIX implementation (Pignatelli et al., 2024), a Markov reward function offers a sparse reward of 1 when the goal is reached and 0 for all other steps. The episode terminates when the maximum number of steps (100) is reached, or the agent collides with an obstacle.

4 EXPERIMENTS

We implement the PPO actor and critic as MLPs with the architecture described in Table 1. Hyperparameters were selected based on a grid search in the region of the baseline presented in the NAVIX Minigrid implementation (Pignatelli et al., 2024).

Table 1: PPO Hyperparameters

Architecture	
Hidden Size	64
Number of Layers	2

Training	
Parallel Environments	16
Steps per Environment	128
Minibatches	8
Epochs	16
Learning Rate	1e-3
GAE λ	0.99
Clip ϵ	0.2
Entropy Coefficient	0.02
Value Function Coefficient	0.5
Max Gradient Norm	0.5

The PPO agent and environment are implemented in JAX (Bradbury et al., 2018). All agents were trained for 5M environment frames on a 24GB Nvidia 4090 GPU, taking between 135 and 170 seconds per agent. We observe that implementing the CC loss and neuron relocation results in a 23% increase in total train time, which, as shown in Figure 2, is primarily due to the

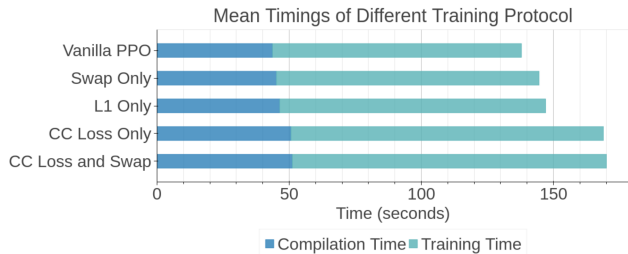


Figure 2: The Impact of our Bio-inspired Training Protocol on Total Training Time, Relative to Vanilla PPO and PPO with L1 Sparsity Baselines.

implementation of the CC loss.

4.1 Emergent Modularity

Figure 3 shows the emergence of two distinct modules within the actor network of a dynamic-obstacles Minigrid agent. As the connection cost weighting factor (λ_{CC}) is increased, independence emerges in the second and third weight layers, with feature-sharing persisting in the first. The neuron relocation results in the input features and output actions reordering in a manner that reflects their relevance, with feature x and y coordinates positioned on the same sides as movements on the x and y axes respectively. Figure 4 shows the necessity of both the connection cost loss and neuron relocation to achieve this result. When L1 sparsity is applied in isolation or with only one of these methods, the same visual clarity is not achieved.

4.2 Module Detection

Modularity within a network can be quantified as the ratio of intra-community links to inter-community links.

$$Q = \frac{1}{2m} \sum_{ij} \left(A_{ij} - \gamma \frac{k_i k_j}{2m} \right) \delta(c_i, c_j) \quad (3)$$

where m is the sum of all edge weights ($m = \sum_{l,ij} w_l^{ij}$), A is the adjacency matrix of the network, k_i is the weighted degree of node i in a null model of the network, and $\delta(c_i, c_j)$ is a binary variable with a value of 1 when i and j belong to the same community. This equation forms the basis of the heuristic Louvain approach to community detection, which iteratively optimises Q through hierarchical local node reassignments (Blondel et al., 2008). The resolution parameter γ influences the size of the detected communities by adjusting the level of connection considered to constitute nodes within the same community.

We apply Louvain clustering to the adjacency matrices of the actor networks in order to automate the identi-

fication of modules and quantify the networks overall modularity. Figure 5a shows the increase in modularity (Q) as the connection cost increases. Empirically, we observe that Q values in the region of 0.4 and above correspond to a visual separation of two modules in the network graph. This begins to occur from λ_{CC} values of 0.0004, and becomes consistent across all random seeds for λ_{CC} values greater than 0.0014. With a λ_{CC} of 0.0014 the mean modularity represents a 340% increase on the baseline value of 0.12 observed with a λ_{CC} of 0. The induced sparsity does, however, impact on performance, as shown in Figure 5b. The decrease in return ranges from 13.7% when modules initially emerge in some seeds to a mean of 20.6% at the stage where modularity occurs consistently. The reduction in performance plateaus between λ_{CC} values of 0.0016 and 0.0026, corresponding to plateaus in both the connection cost loss and the modularity value. This suggests that there is a maximum level of sparsity that can be achieved without a collapse in performance, as begins to occur at $\lambda_{CC} = 0.0028$.

While there is an impact on performance when considering the complete model, the sparsity reduces the proportion of significant weights in the model, consequently allowing for significant pruning. We find that we can remove 85% of the sparse models' parameters without reducing mean performance, compared to 10% in the vanilla PPO-Clip implementation. This may offer further interpretability benefits in addition to significantly reduced computational overhead during inference, as discussed in Appendix B.

Clustering results of the Louvain method are shown in Figure 6 for 4 randomly selected networks with λ_{CC} values between 0.0004 and 0.0008. The Louvain algorithm (Equation 3) does not rely on a predefined number of communities, which offers advantages for scalability to module detection within large networks with an unknown number of modules. However, we observe that the resulting modules do not strongly align with the visually apparent modularity of the networks.

Consequently, we also apply a spectral clustering approach to community detection (von Luxburg, 2007). While spectral clustering techniques are commonly applied to forms of the graph Laplacian, E. Crisostomi and Shorten (2011) demonstrate how clustering of the values of the second eigenvector can be used to identify communities based on the transition matrix of a road network. Following this, we calculate the second eigenvector of the adjacency matrix of the policy network and demonstrate that this shows clustering corresponding to the network modules. Figure 7 shows the result of classifying nodes by partitioning the eigenvector at its largest value separation and shows clear alignment with the visually apparent modularity.

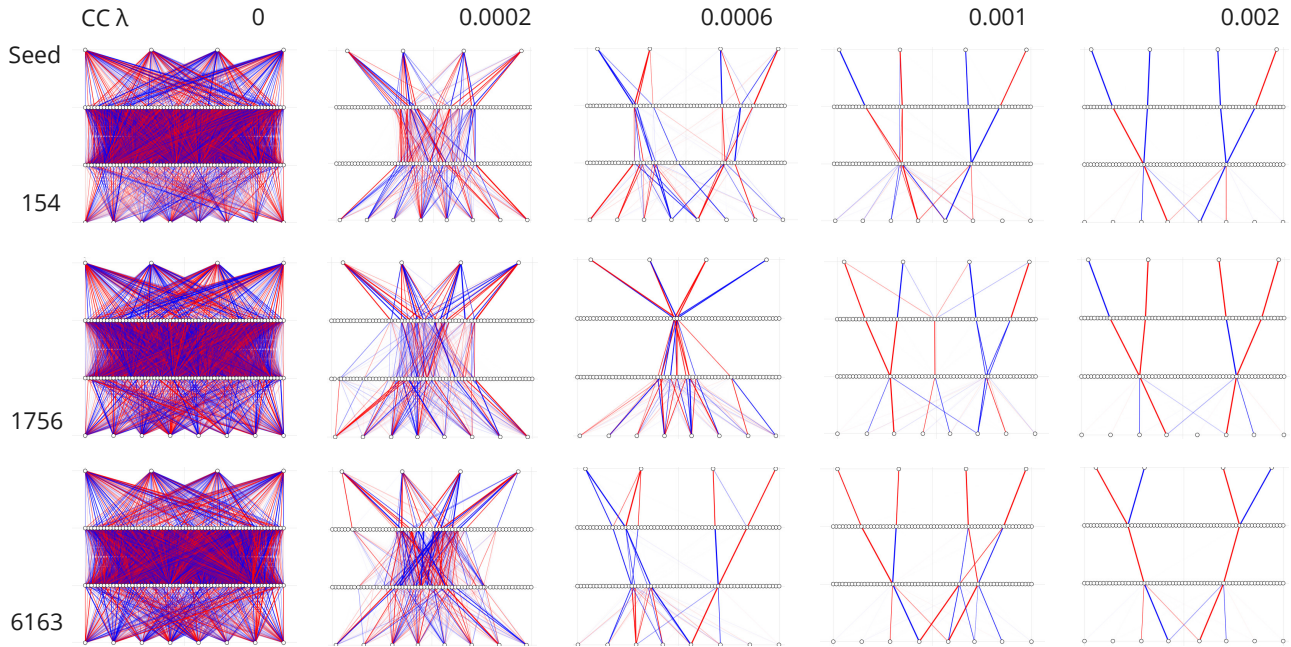


Figure 3: Policy Network Plots Showing the Emergence of Parallel X and Y Processing Modules as the Connection Cost Weighting is Increased for 3 Random Seeds (see Appendix A for Further Examples). Positive and Negative Weights are Shown in Blue and Red Respectively.

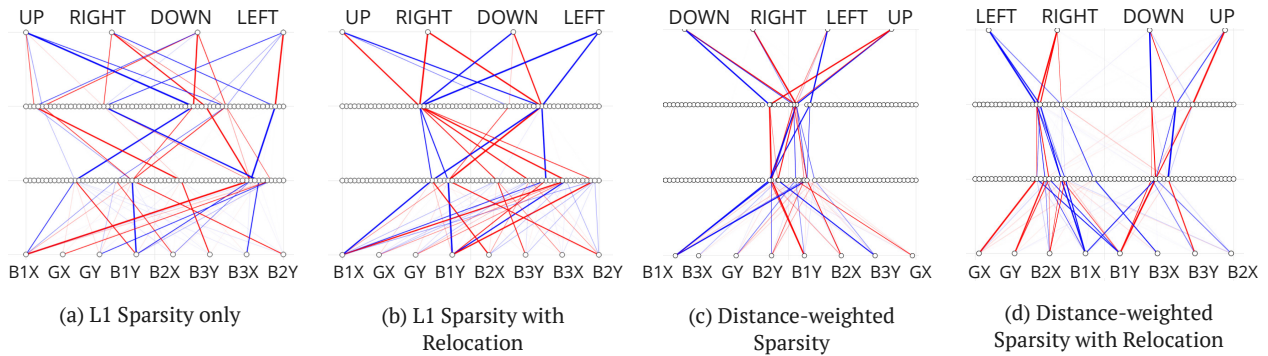


Figure 4: The Impact of Sparsity, Distance Weighting and Neuron Relocation on Visual Modularity.

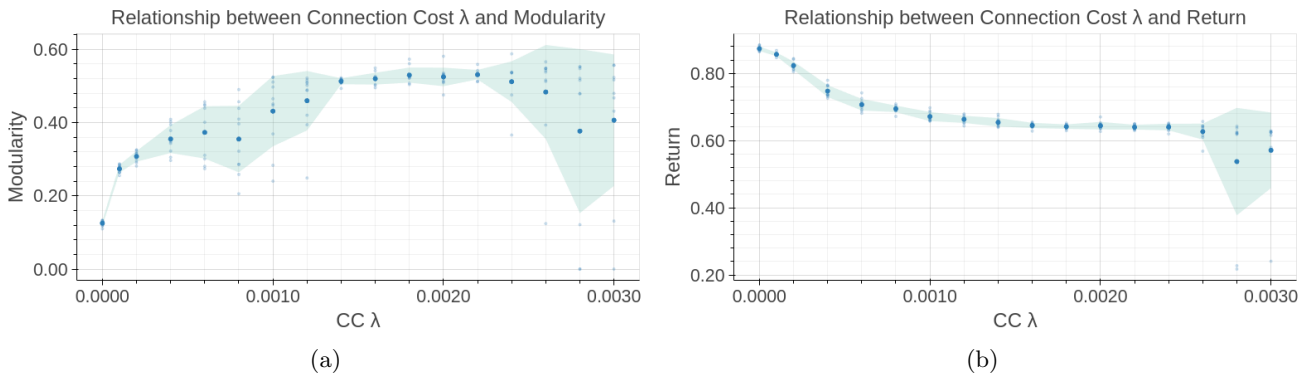


Figure 5: The Impact of Increasing Connection Cost on the Mean and Standard Deviation of (a) Modularity (Q) and (b) Return over 10 Random Seeds.

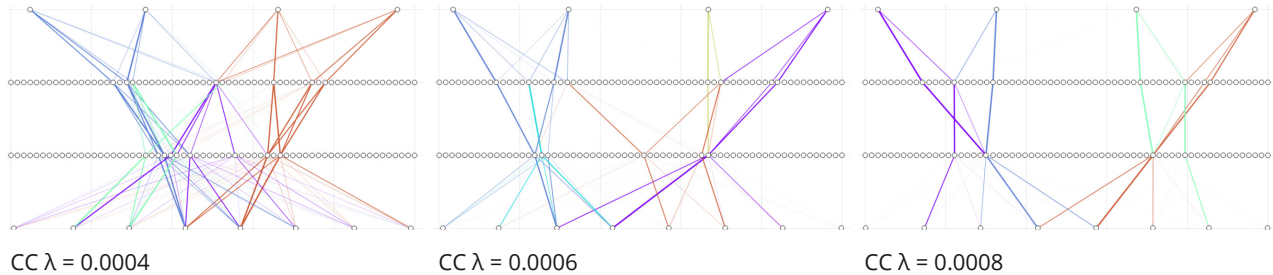


Figure 6: Policy Networks with Louvain Community Detection ($\gamma = 1$).

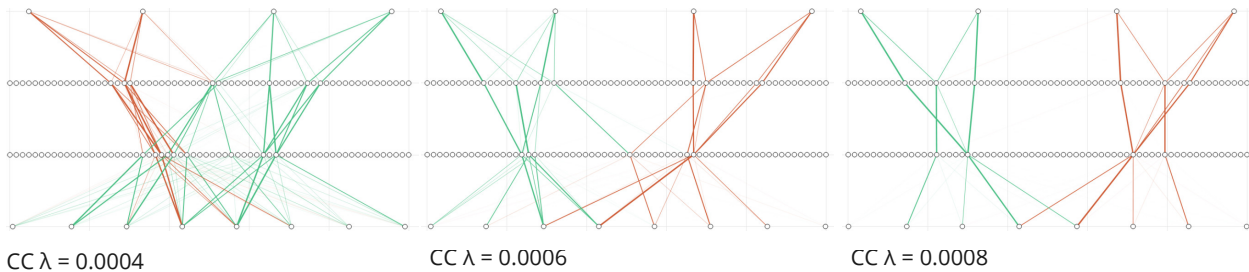


Figure 7: Policy Networks with Community Detection Based on the Second Eigenvector.

In this context, the ability to enforce a desired number of modules afforded by the eigenvector approach offers improves performance over the Louvain method, which subdivides the two visually apparent modules. We hypothesize that this subdivision arises from the lack of intra-layer connections in a neural network, which disrupts the density of the modules and results in a mismatch with the null-model of the network (the random graph model used as a baseline for quantifying the significance of community structures). The development of neural network specific module detection approaches is thus a valuable direction for future work, particularly when considering complex applications where the ability to detect large, unknown numbers of modules is desirable.

4.3 Module Intervention

The automatic classification of neurons into communities enables direct intervention on their behaviour. We achieve this through modification of network parameters prior to inference, which we demonstrate on the eigenvector detected modules of the policy network shown in Figure 8.

Table 2 gives statistics on the actions taken and their outcomes (Failure, Success or Continuation of the episode) for three scenarios: the original network and two modified versions where all weights and biases in the targeted community are masked with a value of

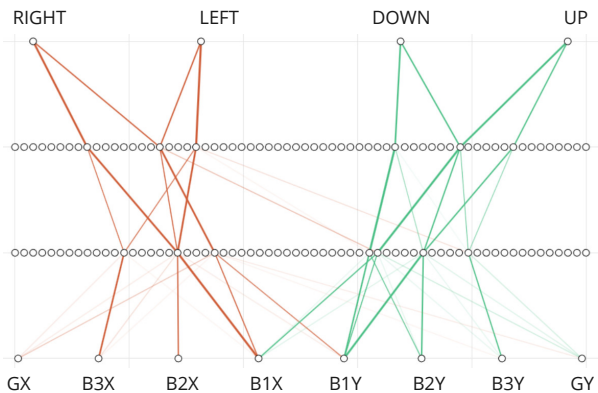


Figure 8: Policy Network ($\lambda_{cc} = 0.0007$) with Eigenvector Based Detection of Community 1 (Red) and Community 2 (Green).

-5. This effectively disables the module and the results show that intervening on community 2 eliminates up and down actions, while the same intervention on community 1 eliminates left and right. Notably, while the success rate drops significantly when a module is masked, the proportion of actions resulting in failures does not increase. This demonstrates that we are able to disable a module while retaining the ability of the other to select the optimal action from its corresponding outputs.

In this example, the module intervention results intu-

Table 2: Action and Action-outcome Distributions over 1000 Episodes for the Network in Figure 8.

Original network				
Returns: 0.688				
	Prop.	Fail	Succ.	Cont.
up	0.24	0.09	0.21	0.7
right	0.25	0.09	0.24	0.66
down	0.24	0.09	0.19	0.72
left	0.26	0.11	0.21	0.68

Community 1 masked				
Returns: 0.151				
	Prop.	Fail	Succ.	Cont.
up	0.49	0.08	0.01	0.91
right	0	-	-	-
down	0.51	0.08	0.01	0.91
left	0	-	-	-

Community 2 masked				
Returns: 0.176				
	Prop.	Fail	Succ.	Cont.
up	0	-	-	-
right	0.53	0.08	0.02	0.91
down	0	-	-	-
left	0.47	0.08	0.02	0.9

itively align with the expected policy behaviour given the task and observed structure of the network visualisations. Moving beyond potentially subjective visual interpretations, it provides an objective validation of module functionality, which becomes increasingly critical when considering scalability. The ability to automatically detect and characterise modules enables the interpretation functional modules in scenarios where visual identification is not feasible due to network size or complexity.

5 CONCLUSIONS

Our results demonstrate that functional modularity can be explicitly encouraged in reinforcement learning through the use training modifications to promote sparsity and locality of connections. To enable scalability to complex decision making applications and model architectures, we propose methods for the automatic detection and characterisation of modules. This functional decomposition enhances interpretability by decomposing the network into distinct, meaningful units which provide insights into the agent’s decision-making process while maintaining a level of abstraction that aligns with human-level understanding.

Several further areas of investigation offer potential to improve the performance and utility of this approach.

Our approaches to module detection present opportunities for refinement, particularly considering scalability to more complex applications. The Louvain approach could be modified to account for the sequentially constrained architecture of neural networks or the spectral clustering approach could be extended to multiple eigenvectors to better capture higher dimensional clusters (von Luxburg, 2007). Alternative methods also merit being explored, such as grouping neurons based on the concurrency of their activations, in order to directly capture functional as opposed to structural modularity. In this work, we characterise modules using parameter modification prior to inference due to its ease of implementation. However, modification of activation values may offer greater insights, particularly for models exhibiting more complex structural modularity, as it offers the potential to intervene on a module while preserving a natural distribution of activation values. The current trade-off between interpretability and performance, while common among ‘white-box’ approaches, is undesirable and a barrier to the adoption of interpretable systems. We expect the specific trade-off between modularity, sparsity, and performance observed here to vary across tasks, but it may be possible to mitigate performance losses, for example by encouraging modularity only in fine-tuning.

Currently, the lack of formal metrics for interpretability make it challenging to comparatively evaluate the utility of differing interpretability approaches, particularly those which approach interpretability at varying levels of abstraction. In the absence of these, we discuss performance, human understanding and scope of our approach, and anticipate evaluating against firm benchmarks as these emerge.

References

- Achterberg, J., Akarca, D., Strouse, D. J., Duncan, J., and Astle, D. E. (2023). Spatially embedded recurrent neural networks reveal widespread links between structural and functional neuroscience findings. *Nature Machine Intelligence*, 5(12):1369–1381.
- Adebayo, J., Gilmer, J., Muelly, M., Goodfellow, I. J., Hardt, M., and Kim, B. (2018). Sanity checks for saliency maps. *CoRR*, abs/1810.03292.
- Amer, M. and Maul, T. (2019). A review of modularization techniques in artificial neural networks. *Artificial Intelligence Review*, 52(1):527–561.
- Atrey, A., Clary, K., and Jensen, D. D. (2019). Exploratory not explanatory: Counterfactual analysis of saliency maps for deep RL. *CoRR*, abs/1912.05743.
- Blondel, V. D., Guillaume, J.-L., Lambiotte, R., and Lefebvre, E. (2008). Fast unfolding of communities

- in large networks. *Journal of Statistical Mechanics: Theory and Experiment*, 2008(10):P10008.
- Bradbury, J., Frostig, R., Hawkins, P., Johnson, M. J., Leary, C., Maclaurin, D., Necula, G., Paszke, A., VanderPlas, J., Wanderman-Milne, S., and Zhang, Q. (2018). JAX: composable transformations of Python+NumPy programs.
- Chevalier-Boisvert, M., Dai, B., Towers, M., de Lazcano, R., Willems, L., Lahlou, S., Pal, S., Castro, P. S., and Terry, J. (2023). Minigrid & miniworld: Modular & customizable reinforcement learning environments for goal-oriented tasks. *CoRR*, abs/2306.13831.
- Coronato, A., Naeem, M., De Pietro, G., and Paragliola, G. (2020). Reinforcement learning for intelligent healthcare applications: A survey. *Artificial Intelligence in Medicine*, 109:101964.
- Doshi-Velez, F. and Kim, B. (2017). Towards a rigorous science of interpretable machine learning. arXiv:1702.08608.
- E. Crisostomi, S. K. and Shorten, R. (2011). A google-like model of road network dynamics and its application to regulation and control. *International Journal of Control*, 84(3):633–651.
- Eppe, M., Gumbsch, C., Kerzel, M., Nguyen, P. D. H., Butz, M. V., and Wermter, S. (2022). Hierarchical principles of embodied reinforcement learning: A review. arXiv: 2012.10147.
- European Commission and High-Level Expert Group on AI (2019). Ethics guidelines for trustworthy artificial intelligence.
- Fodor, J. A. (1985). Précis of the modularity of mind. *Behavioral and Brain Sciences*, 8(1):1–5.
- Gazzaniga, M., Ivry, R., and Mangun, G. (2018). *Cognitive Neuroscience: Fifth International Student Edition*. International student edition. W.W. Norton.
- Glanois, C., Weng, P., Zimmer, M., Li, D., Yang, T., Hao, J., and Liu, W. (2024). A survey on interpretable reinforcement learning. *Machine Learning*, 113(8):5847–5890.
- He, K., Chen, X., Xie, S., Li, Y., Dollár, P., and Girshick, R. (2021). Masked autoencoders are scalable vision learners. arXiv:2111.06377.
- Hein, D., Udluft, S., and Runkler, T. A. (2017). Interpretable policies for reinforcement learning by genetic programming. *CoRR*, abs/1712.04170.
- Jiang, Z. and Luo, S. (2019). Neural logic reinforcement learning. *CoRR*, abs/1904.10729.
- Landajuela, M., Petersen, B. K., Kim, S., Santiago, C. P., Glatt, R., Mundhenk, N., Pettit, J. F., and Faissol, D. (2021). Discovering symbolic policies with deep reinforcement learning. In Meila, M. and Zhang, T., editors, *Proceedings of the 38th International Conference on Machine Learning*, volume 139 of *Proceedings of Machine Learning Research*, pages 5979–5989. PMLR.
- Lipton, Z. C. (2016). The mythos of model interpretability. *CoRR*, abs/1606.03490.
- Liu, Z., Gan, E., and Tegmark, M. (2023). Seeing is believing: Brain-inspired modular training for mechanistic interpretability. arXiv: 2305.08746.
- Lu, R., Li, Y.-C., Li, Y., Jiang, J., and Ding, Y. (2020). Multi-agent deep reinforcement learning based demand response for discrete manufacturing systems energy management. *Applied Energy*, 276:115473.
- Margalit, E., Lee, H., Finzi, D., DiCarlo, J. J., Grill-Spector, K., and Yamins, D. L. (2024). A unifying framework for functional organization in early and higher ventral visual cortex. *Neuron*, 112(14):2435–2451.e7.
- Merel, J., Hasenclever, L., Galashov, A., Ahuja, A., Pham, V., Wayne, G., Teh, Y. W., and Heess, N. (2018). Neural probabilistic motor primitives for humanoid control. *CoRR*, abs/1811.11711.
- Pateria, S., Subagdja, B., Tan, A.-h., and Quek, C. (2021). Hierarchical reinforcement learning: A comprehensive survey. *ACM Comput. Surv.*, 54(5).
- Pignatelli, E., Liesen, J., Lange, R. T., Lu, C., Castro, P. S., and Toni, L. (2024). Navix: Scaling minigrid environments with jax. arXiv:2407.19396.
- Schulman, J., Wolski, F., Dhariwal, P., Radford, A., and Klimov, O. (2017). Proximal policy optimization algorithms. arXiv: 1707.06347.
- Silva, A., Killian, T., Rodriguez, I. D. J., Son, S.-H., and Gombolay, M. (2020). Optimization methods for interpretable differentiable decision trees in reinforcement learning. arXiv: 1903.09338.
- Song, Y., Romero, A., Müller, M., Koltun, V., and Scaramuzza, D. (2023). Reaching the limit in autonomous racing: Optimal control versus reinforcement learning. *Science Robotics*, 8(82).
- Sternberg, S. (2011). Modular processes in mind and brain. *Cognitive Neuropsychology*, 28(3-4):156–208. PMID: 22185235.
- von Luxburg, U. (2007). A tutorial on spectral clustering. *Statistics and Computing*, 17(4):395–416.
- Wang, K., Variengien, A., Conmy, A., Shlegeris, B., and Steinhardt, J. (2022). Interpretability in the wild: a circuit for indirect object identification in gpt-2 small. arXiv: 2211.00593.

Zhang, N., Donahue, J., Girshick, R., and Darrell, T. (2014). Part-based r-cnns for fine-grained category detection. In Fleet, D., Pajdla, T., Schiele, B., and Tuytelaars, T., editors, *Computer Vision – ECCV 2014*, pages 834–849, Cham. Springer International Publishing.

APPENDIX

A Further Modularity Examples

We show further examples of increasing the connection cost over 5 random seeds to demonstrate the consistency with which modularity emerges, and to show the impact on the model architecture when a performance collapse occurs. This can be seen to occur with a connection cost weighting factor, $CC \lambda$, of 0.004.

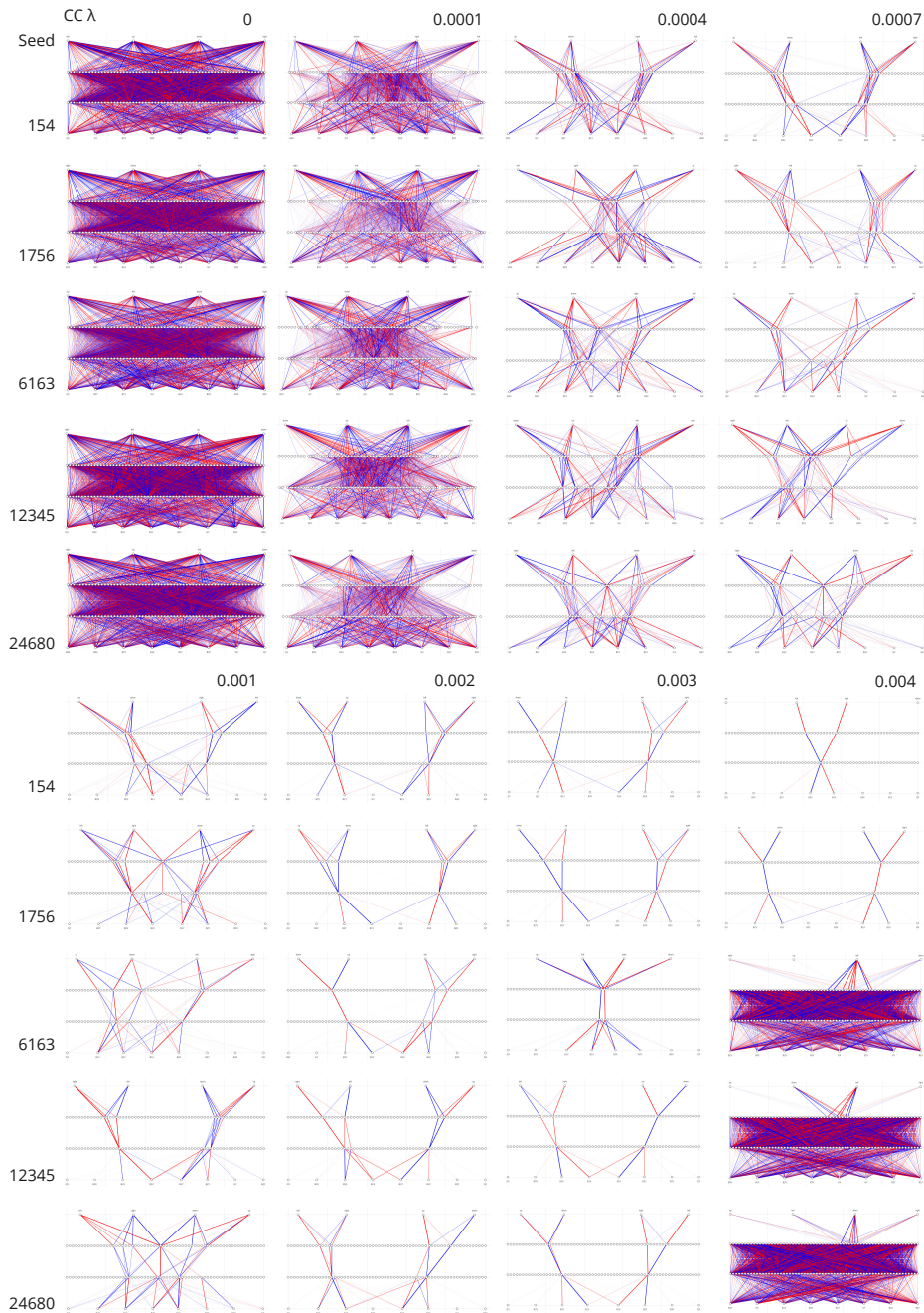


Figure A.1: Further Examples Showing the Impact of Increasing Connection Cost for 5 Random Seeds.

B Pruning Results

We implement parameter pruning based on magnitude by zeroing out a specified fraction of weights and biases with the lowest absolute values in each layer prior to inference. This is done in a layer-wise manner due to the differing distributions of weights and biases across the layers. As illustrated in Figure A.2, models trained with L1 sparsity or our connection cost protocol are highly resilient to pruning and up to 90% of model parameters can be zeroed without a reduction in return. In contrast, models trained with the vanilla PPO implementation exhibit performance degradation when pruning is increased beyond 10%, and by 90% pruning, the performance observed is equivalent to that when actions are selected randomly. This high degree of achievable sparsity presents opportunities for reducing the model memory requirements and increasing the computational efficiency during inference.

We also note that the reduction in performance observed as we increase the weighting of the connection cost loss closely resembles that seen when L1 sparsity is increased, as shown in Figure A.3. Given that L1 sparsity is an established regularisation technique to prevent overfitting, we theorise that our modularity inducing training protocol may offer similar benefits in certain applications.

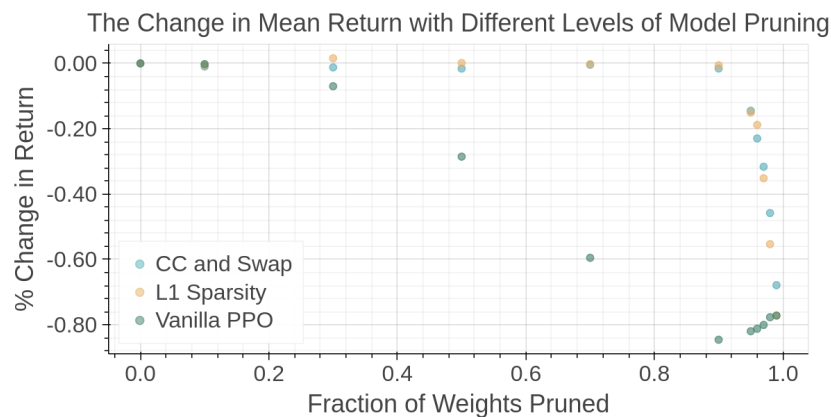


Figure A.2: The Impact of Pruning on Performance of Models with Different Training Protocols

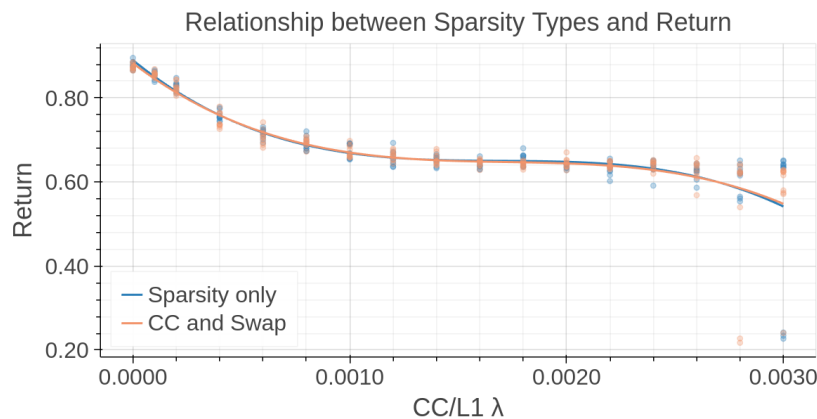


Figure A.3: The Return of Models Trained with L1 Sparsity Compared to our Connection Cost Protocol